A state interaction spin-orbit coupling density matrix renormalization group method

Elvira R. Sayfutyarova and Garnet Kin-Lic Chan

Citation: J. Chem. Phys. **144**, 234301 (2016); doi: 10.1063/1.4953445
View online: http://dx.doi.org/10.1063/1.4953445
View Table of Contents: http://aip.scitation.org/toc/jcp/144/23
Published by the American Institute of Physics

A state interaction spin-orbit coupling density matrix renormalization group method

Elvira R. Sayfutyarova and Garnet Kin-Lic Chan
Department of Chemistry, Princeton University, Princeton, New Jersey 08540, USA

(Received 31 March 2016; accepted 26 May 2016; published online 15 June 2016)

We describe a state interaction spin-orbit (SISO) coupling method using density matrix renormalization group (DMRG) wavefunctions and the spin-orbit mean-field (SOMF) operator. We implement our DMRG-SISO scheme using a spin-adapted algorithm that computes transition density matrices between arbitrary matrix product states. To demonstrate the potential of the DMRG-SISO scheme we present accurate benchmark calculations for the zero-field splitting of the copper and gold atoms, comparing to earlier complete active space self-consistent-field and second-order complete active space perturbation theory results in the same basis. We also compute the effects of spin-orbit coupling on the spin-ladder of the iron-sulfur dimer complex $[Fe_2S_2(SCH_3)_4]^{3-}$, determining the splitting of the lowest quartet and sextet states. We find that the magnitude of the zero-field splitting for the higher quartet and sextet states approaches a significant fraction of the Heisenberg exchange parameter. *Published by AIP Publishing.* [http://dx.doi.org/10.1063/1.4953445]

I. INTRODUCTION

Spin-orbit coupling (SOC) derives from the coupling of the electron spin to the magnetic fields induced by the relative motion of other charges. As SOC increases with nuclear charge, it plays a particularly important role in molecules containing heavy atoms such as transition metals, and is the dominant spin-dependent relativistic effect.[1–4] When there are nearly degenerate electronic states of different multiplicity, even a small SOC matrix element can strongly mix the states. In such cases, correctly treating the SOC is crucial to obtain even a qualitative understanding of the electronic structure.

Electronic near-degeneracy is also closely associated with nondynamic correlation. This type of correlation is also known as strong correlation, as in this situation the Coulomb interaction matrix element becomes large compared to the single-particle energy splitting. Much work has been devoted in the last decade to finding more efficient methods to treat strong correlation when the number of near-degenerate frontier orbitals is large. An advance in this direction has been provided by the *ab-initio* density matrix renormalization group (DMRG).[5–52] Using the *ab-initio* DMRG, it is now routine to treat active spaces far in excess of the 16 orbital limit of earlier complete active space methods. In transition metal systems, active spaces with up to 50 orbitals can be routinely converged to chemical accuracy.[26,28,29,31,34,35,38–41,43,44,48]

In this work, we describe a method to combine a treatment of spin-orbit coupling with a density matrix renormalization group description of the electronically near-degenerate individual states. We use a state interaction approach,[53–58] whereby DMRG wavefunctions are determined for spin-pure electronic states, and the Hamiltonian with spin-orbit coupling is recomputed within this basis and diagonalized. The spin-orbit coupling operator is approximated within the spin-orbit mean-field approximation.[59–61] A related state-interaction DMRG approach to the spin-orbit coupling, as applied to g-tensors, has been presented by Roemelt in Ref. 62. However, we use a different approach than Ref. 62 to represent the spin-pure electronic states. In particular, we do not assume that different states share the same DMRG renormalized basis. This allows for a more flexible and accurate representation of the individual spin-coupled states for a given DMRG bond-dimension, at a slightly higher cost.

We use our method to compute zero-field splittings (ZFS), i.e., the splitting of the spin multiplets due to the relativistic spin-orbit interaction, in the Cu and Au atoms using basis sets of up to augmented double-zeta with polarization quality, and correlating all electrons outside of a Ne and Kr core, respectively, converging splitting energies to sub-milli-Hartree accuracy. The resulting zero-field splittings are in excellent agreement with experiment. We also compute the ZFS in a more complex molecule, the $[Fe_2S_2(SCH_3)_4]^{3-}$ dimer, where we obtain the magnitude of the zero-field splittings of the low-lying spin states. Intriguingly, the observed ZFSs in the higher spin states are a significant fraction of the Heisenberg exchange parameter.

II. THEORY

We start with the definition of the relativistic Hamiltonian. The most complete description of relativistic effects found in molecular quantum chemistry calculations is given by the four-component relativistic Dirac-Coulomb-Breit Hamiltonian.[2,63–66] (This Hamiltonian has recently been used with the DMRG as discussed in Ref. 47.) However, four-component methods remain computationally expensive for practical calculation, and simpler approximations are often used. The Breit-Pauli approximation[64,67–69] reduces the four-component relativistic Dirac-Coulomb-Breit Hamiltonian[2,63–66] to two-component form, with a large number of terms. It is common to divide these terms into two sets, spin-independent

and spin-dependent. The latter includes electronic spin-spin coupling and nuclear hyperfine interactions, as well as the SOC interaction. Since SOC effects are generally at least an order of magnitude larger than those due to spin-spin coupling, and nuclear magnetic interactions are several orders of magnitude weaker than even the spin-spin coupling, we only treat the SOC in this work, and do not consider the other interactions. In light of this, the Hamiltonian can be represented as

$$\hat{H} = \hat{H}_{\mathrm{SR}} + \hat{H}_{\mathrm{SO}}, \tag{1}$$

where $\hat{H}_{\mathrm{SR}}$ is the non-relativistic part of the Hamiltonian plus spin-independent scalar relativistic effects such as the mass-velocity contribution, while $\hat{H}_{\mathrm{SO}}$ is the spin-dependent part of the Hamiltonian, such as the spin-orbit coupling operator. In this work, we use the 2nd order Douglas-Kroll-Hess approximation $\hat{H}_{\mathrm{SR}} = \hat{H}_{\mathrm{DKH2}}$[70–76] to include scalar relativistic effects for the Cu and Au atoms, and the Born-Oppenheimer non-relativistic Hamiltonian $\hat{H}_{\mathrm{SR}} = \hat{H}_{\mathrm{BO}}$ for the $[Fe_2S_2(SCH_3)_4]^{3-}$ dimer. For $\hat{H}_{\mathrm{SO}}$ we use the spin-orbit mean-field approximation, $\hat{H}_{\mathrm{SOMF}}$[59–61] (see below for definition).

$\hat{H}$ does not commute with the $\hat{S}^2$ and $\hat{S}_z$ spin operators. This is what gives rise to the zero-field splitting of the spin-manifolds of interest in this work. On the other hand, $\hat{H}_{\mathrm{SR}}$, which only includes the scalar relativistic effects, does commute with the spin operators. There are thus two basic routes to determine the ZFS. The first, one-step, spin-orbit coupling treatment directly diagonalizes $\hat{H}$ in a basis which does not assume spin symmetry.[77–79] The second, two-step, state-interaction method expands the eigenstates of $\hat{H}$ in terms of the spin-pure eigenstates of $\hat{H}_{\mathrm{SR}}$.[53,54,80,81] The coefficients of expansion may be determined using different methods, such as perturbation theory[82–86] or through diagonalization (state interaction).[54–58] The latter corresponds to solving

$$\mathbf{Hc} = E\mathbf{Sc} \tag{2}$$

with matrix elements $H_{IJ} = \langle\Psi_I|\hat{H}|\Psi_J\rangle$, $S_{IJ} = \langle\Psi_I|\Psi_J\rangle$ where $|\Psi_I\rangle$, $|\Psi_J\rangle$ are eigenstates of $\hat{H}_{\mathrm{SR}}$. (The overlap matrix is only required if ground-state orthogonality is not imposed when determining excited states in the DMRG.)

The performance of one- and two-step methods depends on the interplay between electron correlation and SOC. In lighter atoms and molecules, these two effects are largely uncoupled and SOC mostly influences the fine-structure in the spectra; therefore they can be treated in two different steps, and typically only a modest number of expansion functions are needed. In systems with very heavy elements, electron correlation and spin-orbit coupling are of the same order of magnitude and more care is needed. When using the two-step method for heavy elements, scalar relativistic corrections must be added to the electronic Hamiltonian in the first step, and a sufficient number of eigenstates of $\hat{H}_{\mathrm{SR}}$ must be used in the second step. Note that with an infinite set of expansion functions $|\Psi_I\rangle$, the two-step and one-step methods give the same result; the error in the two-step method arises from the truncation of the set of interacting states.

In this work, we use the two-step state-interaction diagonalization method to treat spin-orbit coupling and compute the zero-field splitting. The eigenstates of $\hat{H}_{\mathrm{SR}}$ are approximated as density matrix renormalization group (DMRG) (also known as matrix product state (MPS)) wavefunctions. The simplest way to represent multiple states within the DMRG formalism is to assume that different states share the same renormalized basis. Roemelt has recently used this DMRG representation, in conjunction with the two-step state-interaction method, to compute molecular g-tensors.[62] In this work, we implement a more flexible (though also slightly more expensive) approach where the DMRG states are not assumed to share the same renormalized basis. This is useful in reaching higher accuracy and in cases where states of different spin have very different electronic structure.

The basic task is to define the procedure to compute the matrix elements of $\hat{H}$ and $\hat{S}$ between the arbitrary DMRG states appearing in Eq. (2). Using the spin-orbit mean-field approximation for $\hat{H}_{\mathrm{SO}}$ this amounts to the simple problem of computing single-particle transition density matrices. Below, we first define the spin-orbit mean-field approximation $\hat{H}_{\mathrm{SOMF}}$ used in the work, and then describe the implementation of the matrix element computation.

A. Spin-orbit mean-field approximation

The Breit-Pauli spin-orbit Hamiltonian is a two-particle operator and can be written as[1,59,87]

$$\hat{H}_{\mathrm{SO}} = \hat{H}^{(1)}_{\mathrm{SO}} + \hat{H}^{(2)}_{\mathrm{SO}} = \sum_i \hat{\mathbf{h}}_i \cdot \hat{\mathbf{s}}_i + \sum_i \sum_{j\neq i} \hat{\mathbf{g}}_{ij} \cdot \left(\hat{\mathbf{s}}_i + 2\hat{\mathbf{s}}_j\right) \tag{3}$$

with the one- and two-electron operators being defined by

$$\hat{\mathbf{h}}_i = \frac{\alpha^2}{2} \sum_A Z_A r_{iA}^{-3} \hat{\mathbf{l}}_{iA}, \tag{4}$$

$$\hat{\mathbf{g}}_{ij} = -\frac{\alpha^2}{2} \hat{\mathbf{l}}_{ij} r_{ij}^{-3}, \tag{5}$$

where α is the fine structure constant, $\hat{\mathbf{r}}_i$, $\hat{\mathbf{p}}_i$, $\hat{\mathbf{s}}_i$ represent the position, momentum, and spin operators of the ith electron, $r_{ij} = |\hat{\mathbf{r}}_{ij}| = |\hat{\mathbf{r}}_i - \hat{\mathbf{r}}_j|$ is the distance between electrons i and j, $\hat{\mathbf{l}}_{ij} = \hat{\mathbf{r}}_{ij} \times \hat{\mathbf{p}}_i$ is the angular momentum of the ith electron relative to the electron j and similarly, $\hat{\mathbf{l}}_{iA} = \hat{\mathbf{r}}_{iA} \times \hat{\mathbf{p}}_i$ is the angular momentum of the ith electron relative to the nucleus A with $r_{iA} = \left|\hat{\mathbf{r}}_i - \hat{\mathbf{R}}_A\right|$ being the distance between them, and Z_A denotes the nuclear charge of the Ath nucleus.

The spin-orbit mean-field Hamiltonian amounts to simplifying $\hat{H}_{\mathrm{SO}}$ into an effective single-particle operator, $\hat{H}_{\mathrm{SOMF}}$.[60,61] This approximation has been shown to yield small errors in a variety of applications.[60,61,88–91] The SOMF Hamiltonian introduces two main approximations. First, it neglects the effect of mutually doubly excited configurations (i.e., matrix elements connecting determinants that are doubly excited with respect to each other) as they usually contribute less than 1% to the total SOC matrix element between two states.[60,88,90] Second, the two-electron spin-orbit interactions from Eq. (5) are averaged over α and β spin orientations before the spin integration. This leads to the effective spin-orbit matrix element between orbitals i and j,

$$\langle i|\hat{H}_{\mathrm{SOMF}}|j\rangle = \langle i|\hat{H}^{(1)}_{\mathrm{SO}}|j\rangle + \sum_{kl} D_{kl} \times \left\{\langle ik|\hat{H}^{(2)}_{\mathrm{SO}}|jl\rangle - \frac{3}{2}\langle ik|\hat{H}^{(2)}_{\mathrm{SO}}|lj\rangle - \frac{3}{2}\langle ki|\hat{H}^{(2)}_{\mathrm{SO}}|jl\rangle\right\}. \quad (6)$$

The summation in Eq. (6) runs over *all* spatial molecular orbitals and D_{kl} is the single-particle density matrix element. In the original derivation, this density matrix is assumed idempotent. Here, we use the density matrix of the reference ground-state which is not necessarily idempotent. The above reduction to single-particle form can be further improved. For example, in Ref. 92, it is argued that for high-spin systems ($S > 1/2$) there is an additional non-negligible contribution $\frac{1}{2}\sum_{mn} D_{mn}\langle im|\hat{H}^{(2)}_{\mathrm{SO}}|jn\rangle$, where m,n are the singly occupied orbitals. We have not considered these enhancements here.

The SOMF Hamiltonian is a single-particle Hamiltonian. In second quantization, we can rewrite it as[53,61]

$$\hat{H}_{\mathrm{SOMF}} = \sum_{ij}\left(V^x_{ij}\hat{T}^x_{ij} + V^y_{ij}\hat{T}^y_{ij} + V^z_{ij}\hat{T}^z_{ij}\right), \quad (7)$$

where $V^{x,y,z}_{ij}$ is an effective set of one-electron integrals,

$$\langle i|\hat{\mathbf{V}}|j\rangle = \langle i|\hat{\mathbf{h}}_1|j\rangle + \sum_{kl} D_{kl} \times \left\{\langle ik|\hat{\mathbf{g}}_{12}|jl\rangle - \frac{3}{2}\langle ik|\hat{\mathbf{g}}_{12}|lj\rangle - \frac{3}{2}\langle ki|\hat{\mathbf{g}}_{12}|jl\rangle\right\} \quad (8)$$

and $\hat{T}^{x,y,z}_{ij}$ represent the Cartesian triplet excitation operators,

$$\hat{T}^x_{ij} = \frac{1}{2}\left(a^\dagger_{i\alpha}a_{j\beta} + a^\dagger_{i\beta}a_{j\alpha}\right), \quad (9)$$

$$\hat{T}^y_{ij} = \frac{1}{2i}\left(a^\dagger_{i\alpha}a_{j\beta} - a^\dagger_{i\beta}a_{j\alpha}\right), \quad (10)$$

$$\hat{T}^z_{ij} = \frac{1}{2}\left(a^\dagger_{i\alpha}a_{j\alpha} - a^\dagger_{i\beta}a_{j\beta}\right). \quad (11)$$

The Cartesian triplet operators are related to triplet operators in the spin-tensorial form via the linear transformation[93]

$$\left(\hat{T}^x,\hat{T}^y,\hat{T}^z\right) = \left(\hat{T}^{1,1},\hat{T}^{1,-1},\hat{T}^{1,0}\right)\begin{pmatrix} -\frac{1}{2} & -\frac{1}{2i} & 0 \\ \frac{1}{2} & -\frac{1}{2i} & 0 \\ 0 & 0 & \frac{1}{\sqrt{2}} \end{pmatrix}. \quad (12)$$

The spin-tensorial form of $\hat{H}_{\mathrm{SOMF}}$ can be used directly in a spin-adapted algorithm, such as the spin-adapted DMRG algorithm that we use in this work.

B. Matrix element evaluation with DMRG/MPS wavefunctions

We now describe the evaluation of matrix elements with DMRG/MPS wavefunctions. Additional details on the DMRG can be obtained from several articles and reviews.[5–52,94,95]

In the DMRG, the orbitals (sites) are arranged as a one-dimensional lattice. Given a set of well-ordered N orbitals,[8,12,15,19,20,27,32,36,52,96,97] the DMRG wavefunction (also known as a matrix product state (MPS)) can be expressed as

$$|\Psi\rangle = \sum_{\{n\}} \mathbf{L}^{n_1}\ldots\mathbf{L}^{n_{i-1}}\ldots\mathbf{C}^{n_i}\ldots\mathbf{R}^{n_{i+1}}\ldots\mathbf{R}^{n_N}|n_1\ldots n_N\rangle, \quad (13)$$

where for a given occupation string n, $\mathbf{L}^n$, $\mathbf{C}^n$, $\mathbf{R}^n$ are $M\times M$ matrices, with the leftmost and rightmost boundary matrices being $1\times M$ row and $M\times 1$ column vectors, respectively. The dimension M is known variously as the number of renormalized states (in DMRG language) or, the bond dimension of the state (in MPS language). The product structure of the state leads to redundant "gauge" degrees of freedom. We have fixed this degeneracy in Eq. (13) by working on the site i canonical form. This imposes left- and right-orthogonality conditions on the $\mathbf{L}^n$ and $\mathbf{R}^n$ matrices to the left and right of site i, i.e., $\sum_n (\mathbf{L}^n)^\dagger\mathbf{L}^n = 1$, $\sum_n \mathbf{R}^n(\mathbf{R}^n)^\dagger = 1$. With these conditions, the $\mathbf{L}^n$ and $\mathbf{R}^n$ matrices are known as left- and right-rotation matrices, while $\mathbf{C}^n$ is termed the wavefunction matrix. Eq. (13), where the wavefunction matrix is associated with a single site, represents the "one dot" or "one site" form of the DMRG wavefunction. This is the form that we assume in our current implementation of spin-orbit coupling matrix elements.

A DMRG calculation involves optimizing the matrices appearing in Eq. (13). Because this optimization is carried out one matrix (site) at a time, the optimization takes the form of a sweep over the orbitals. When a single state is optimized the choice of site i in the canonical form in Eq. (13) is arbitrary, as one can convert the canonical form at site i to the form at any other site. In the canonical form, it is convenient to express the DMRG wavefunction in terms of a renormalized many particle basis,

$$|\Psi\rangle = \sum_{lnr} C^n_{lr}|lnr\rangle, \quad (14)$$

where $\{|l\rangle\}$ and $\{|r\rangle\}$ are orthonormal left and right renormalized many-particle basis states, defined through the $\mathbf{L}^n$ and $\mathbf{R}^n$ matrices,

$$|l\rangle = \sum_{\{n\}}(\mathbf{L}^{n_1}\ldots\mathbf{L}^{n_{i-1}})_l|n_1\ldots n_{i-1}\rangle, \quad (15)$$

$$|r\rangle = \sum_{\{n\}}(\mathbf{R}^{n_{i+1}}\ldots\mathbf{R}^{n_N})_r|n_{i+1}\ldots n_N\rangle, \quad (16)$$

and $\{|n\rangle\}$ are the states in the Fock space of site i. For convenience, we can also group the state of site i with either the left or right renormalized block basis, writing, e.g.,

$$|\Psi\rangle = \sum_{lnr} C^n_{lr}|lnr\rangle = \sum_{dr} C_{dr}|dr\rangle, \quad (17)$$

where here we have grouped site i with the left block of sites. During the sweep, the canonical form is moved from one site to the next, while the coefficients C_{dr} at each site are optimized.

In a spin-adapted DMRG algorithm, $|l\rangle$, $|n\rangle$, and $|r\rangle$ are spin-pure eigenstates of the $\hat{S}^2$ and $\hat{S}_z$ spin operators acting on the sets of sites $1\ldots i-1$, i, and $i+1\ldots N$, respectively, and the total wavefunction $|\Psi\rangle$ recouples these into a spin-pure state for the whole lattice.[35,98,99] It is sufficient then to work only with the multiplet space rather than the state space, and individual $2S+1$ spin states and their matrix elements can be regenerated using Clebsch-Gordon coefficients and

the Wigner-Eckart theorem. The reduced wavefunction in the multiplet space is written as

$$\|\Psi_S\rangle = \sum_{dS_d rS_r} C^S_{dS_d rS_r} \|dS_d rS_r\rangle, \tag{18}$$

where S is the total spin irrep of the state, dS_d, rS_r denote multiplets with spin irreps S_d and S_r associated with the left (plus dot) and right blocks, respectively.

In a DMRG calculation to optimize multiple eigenstates of the Hamiltonian, there are different choices for how to treat the different matrices appearing in Eq. (13). In the simplest case, namely state-averaged DMRG calculations, the left and right renormalization matrices, $\mathbf{L}^n$ and $\mathbf{R}^n$, are held the same for all eigenstates, and only the wavefunction matrix $\mathbf{C}^n$ differs between states. Because of the constraint that the left and right matrices are shared between the Hamiltonian eigenstates, the canonical forms at different sites (under this constraint) are no longer equivalent. Thus, one must specify the particular site i associated with the wavefunction matrix that is used to compute expectation values. The wavefunction matrix is typically taken to be at the center of the lattice, where it has the largest number of degrees of freedom. This state-averaged DMRG representation was used by Roemelt to compute spin-orbit coupling matrix elements in Ref. 62. While it allows for maximal reuse of intermediates in the DMRG calculation, it is not the most flexible choice to accurately represent an individual state (for example, in the computation of zero-field splittings). Greater flexibility is provided instead by a state-specific approach that allows arbitrary DMRG wavefunctions to represent each Hamiltonian eigenstate. This means that different eigenstates have different sets of $\mathbf{L}^n$, $\mathbf{R}^n$, and $\mathbf{C}^n$ matrices. The relative computational merits of the two approaches are system dependent. For example, the state-averaged approach allows all spin-orbit coupling matrix elements between two states to be computed in a single sweep, while the state-specific approach would require $O(N^2_{eig})$ sweeps, where N_{eig} is the number of Hamiltonian eigenstates considered. However, the state-averaged approach requires a larger bond dimension to accurately represent each state. The loss of accuracy relative to the state-specific approach depends on the relative similarity in electronic structure between different Hamiltonian eigenstates.

In this work, we have implemented the general state-specific algorithm where we do not need to impose the condition of shared DMRG renormalization matrices between states. The matrix element $\langle\Psi_I|\hat{H}_{\mathrm{SOMF}}|\Psi_J\rangle$ requires one-particle reduced density matrix elements $\langle\Psi_I|\hat{\mathbf{T}}^1_{ij}|\Psi_J\rangle$ between arbitrary matrix product states. In addition, for the eigenvalue equation (2), we require the matrix elements $\langle\Psi_I|\hat{H}_{\mathrm{SR}}|\Psi_J\rangle$ (and $\langle\Psi_I|\Psi_J\rangle$ also if orthogonality is not imposed in determining the excited states). To efficiently compute the spin-conserving $\langle\Psi_I|\hat{H}_{\mathrm{SR}}|\Psi_J\rangle$ matrix elements we use the standard sweep procedure, where we evaluate and store transition renormalized operators. These are defined such that the left (right) renormalization involves two different sets of left (right) rotation matrices $\mathbf{L}^n_I$ ($\mathbf{R}^n_J$) from $\langle\Psi_I|$ and $|\Psi_J\rangle$, respectively. Otherwise, the algorithm is the same as the usual density matrix sweep evaluation, as described, for example, in Ref. 35.

In the case of the SOMF expectation value, we need to additionally consider a one-particle RDM element which changes the total spin. We first express the triplet tensor operator, $\hat{\mathbf{T}}^1_{ij}$ ($\hat{\mathbf{B}}^1_{ij}$ in Ref. 35), in terms of operators acting on the left (plus dot) and right blocks, respectively (left-right decomposition),

$$\hat{\mathbf{T}}^1_{ij}[dr] = \begin{cases} \hat{\mathbf{T}}^1_{ij}[d]\otimes_1\hat{\mathbf{1}}[r], & ij \in d \\ a^{\dagger,1/2}_i[d]\otimes_1 a^{1/2}_j[r], & i \in d, j \in r, \\ \hat{\mathbf{1}}[d]\otimes_1\hat{\mathbf{T}}^1_{ij}[r], & ij \in r \end{cases} \tag{19}$$

where $\otimes_1$ indicates that the $S = 1$ component of the tensor product is taken. We then compute the action of $\hat{\mathbf{T}}^1_{ij}$ on the reduced wavefunction using the analogue of Eq. (35) in Ref. 35, where the $9j$ symbol is modified to take into account the triplet nature of the operator,

$$C^{S',ij}_{d'S'_d,rS'_r} = \sum_{S_d S_r} \begin{bmatrix} S_r & S_d & S \\ S^O_r & S^O_d & 1 \\ S'_r & S'_d & S' \end{bmatrix} \langle d'S'_d\|\hat{\mathbf{O}}^{S^O_d}_d\|dS_d\rangle \times \langle r'S'_r\|\hat{\mathbf{O}}^{S^O_r}_r\|rS_r\rangle C^S_{dS_d,rS_r} \tag{20}$$

where the operators $\hat{\mathbf{O}}^{S^O_d}_d$ and $\hat{\mathbf{O}}^{S^O_r}_r$ are the components of $\hat{\mathbf{T}}^1_{ij}$ appearing in Eq. (19). The reduced matrix element of $\hat{\mathbf{T}}^1_{ij}$ is then obtained as

$$\langle\Psi_{I,S'}\|\hat{\mathbf{T}}^1_{ij}\|\Psi_{J,S}\rangle = \sum_{S'_d S'_r} C^{S',ij*}_{d'S'_d,r'S'_r} C^S_{d'S'_d,r'S'_r}. \tag{21}$$

From these reduced matrix elements, we can regenerate the full matrix elements with $3j$-symbols through

$$\langle\Psi_{I,S'M'_S}|\hat{T}^{1,M}_{ij}|\Psi_{J,SM_S}\rangle = (-1)^{S'-M'_S} \begin{pmatrix} S' & 1 & S \\ -M'_S & M & M_S \end{pmatrix} \times \langle\Psi_{I,S'}\|\hat{\mathbf{T}}^1_{ij}\|\Psi_{J,S}\rangle. \tag{22}$$

C. State interaction algorithm summary

Using the implementation described above, the spin-orbit state-interaction algorithm is summarized as follows:

1. Solve for eigenstates of $\hat{H}_{\mathrm{SR}}$ using DMRG (state-averaged or state-specific or combinations of both). If necessary, compute the additional matrix elements $\langle\Psi_I|\hat{H}_{\mathrm{SR}}|\Psi_J\rangle$ and $\langle\Psi_I|\Psi_J\rangle$.
2. Build the matrix elements of $\hat{H}_{\mathrm{SOC}}$ between all the DMRG wavefunctions from the triplet transition density matrix.
3. Diagonalize Eq. (2) to obtain the ZFS and SOC wavefunctions.

III. RESULTS AND DISCUSSION

We have implemented the state-interaction SO coupling scheme within the Block program. The SOC integrals $\langle i \mid \hat{\mathbf{1}}_{1A} r^{-3}_{1A} \mid j\rangle$ and $\langle ik \mid \hat{\mathbf{1}}_{12} r^{-3}_{12} \mid jl\rangle$ were implemented in terms of differentiated Coulomb integrals following Refs. 100 and 101.

All DMRG calculations were spin-adapted and were performed using the Block code with orbitals starting either

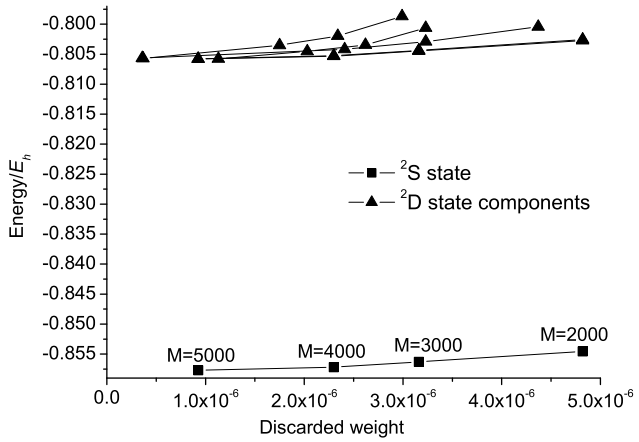

FIG. 1. Energy (E+1653) in E_h and discarded weights of a spin-adapted DMRG calculation on the ^{2}S and ^{2}D states of the copper atom.

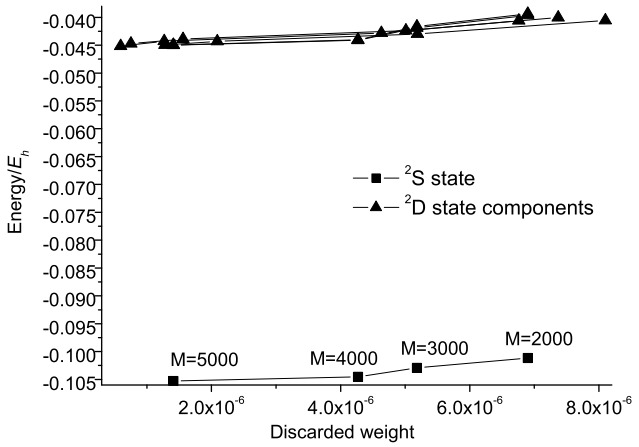

FIG. 2. Energy (E+18 994) in E_h and discarded weights of a spin-adapted DMRG calculation on the ^{2}S and ^{2}D states of the gold atom. Basis I.

from complete active space self-consistent field (CASSCF) or from unrestricted Kohn-Sham (UKS) calculations. For the copper and gold atoms the initial CASSCF calculations were carried out using the Molpro package;[102] the UKS calculations with orbital localization for the iron-sulfur complex were performed using PySCF.[103] SOC integrals were obtained from PySCF and its interface to Block and Molpro.

A. Copper atom

We computed the ZFS between the $^2S_{1/2}$ Cu ground state corresponding to the $3d^{10}4s^1$ configuration and the $^2D_{5/2}$ and $^2D_{3/2}$ states associated with the $3d^94s^2$ configuration, using the ANO-RCC[104] basis set, contracted to 6s5p3d2f.

First, state-averaged CASSCF with an 11 orbital active space (consisting of the $3d$, $3d'$, and $4s$ shells), with scalar relativistic corrections from the second order Douglas-Kroll-Hess Hamiltonian, was used to optimize the orbitals of the ground state and the five components of the ^{2}D multiplet within D_{2h} point group symmetry. We used equal weights for both states, i.e., 0.5 for the ground ^{2}S state and 0.5 for the ^{2}D multiplet. The $3d'$ orbitals provide "double shell" correlations[105–107] that are needed to accurately describe the energy separation between states with different $3d$ and $4s$ occupations in first-row transition metal systems.

Next, DMRG calculations were performed using the state-averaged orbitals from CASSCF to compute all components of the ^{2}D state and the ^{2}S state and subsequently evaluate the transition RDMs and the matrix elements of $\hat{H}$ between them. The $1s, 2s, 2p$ orbitals were treated as frozen core, and all other orbitals were correlated, thus the space treated in the DMRG consisted of 19 electrons and 45 orbitals with the ANO-RCC basis. The DMRG energy for each state was converged to better than $10^{-3}E_h$ accuracy using a bond-dimension of $M = 5000$. A convergence plot of the state energies with the DMRG discarded weight (largest discarded weight in the last sweep)[52] is shown in Fig. 1.

The computed spin-orbit coupled energy levels (relative to the ground-state) are presented in Table I along with the earlier CASSCF and CASPT2 results of Ref. 53, and the experimental levels. The $^2D_{5/2} - {}^2D_{3/2}$ splitting is essentially the same for all the methods and in perfect agreement with experiment. The $^2D_{5/2}$ and $^2D_{3/2}$ excitation energies, however, differ between the methods. Note that the difference (0.08 eV) between the CASSCF results obtained here and those of Ref. 53 with the same basis set is likely due to the use of state-averaged versus state-specific orbitals. Both state-averaged and state-specific (11e,11o) CASSCF-SO calculations find a ^{2}D excitation more than 0.10 eV above the experimental value. The (19e,45o) DMRG-SISO energy levels and the earlier (11e,11o) CASPT2-SO results of Ref. 53 are both in improved agreement with experiment; in the case of DMRG-SISO, the $^2D_{5/2}$ and $^2D_{3/2}$ excitations are 0.08 and 0.07 eV lower than experiment, while CASPT2-SO overestimates them by 0.04 and 0.05 eV, respectively.

B. Gold atom

Similar calculations were performed for the Au atom. The energy separation between the ground state $^2S_{1/2}$ (corresponding to the $5d^{10}6s^1$ configuration) and the $^2D_{5/2}$

TABLE I. The $3d^{10}4s^1$–$3d^94s^2$ energy separation in the Cu atom (in eV).

Term	CASSCF-SO (11e,11o)	CASSCF-SO (11e,11o)[a]	CASPT2-SO (11e,11o)[a]	DMRG-SISO (19e,45o)[b]	Expt.[108]
$^2D_{5/2}$	1.57	1.49	1.43	1.31	1.39
$^2D_{3/2}$	1.83	1.75	1.69	1.57	1.64
$^2D_{5/2}-{}^2D_{3/2}$	0.26	0.26	0.26	0.26	0.25

[a]State-specific CASSCF and CASPT2 from Ref. 53 using the same basis set.
[b]Using state-averaged (11e,11o) CASSCF orbitals.

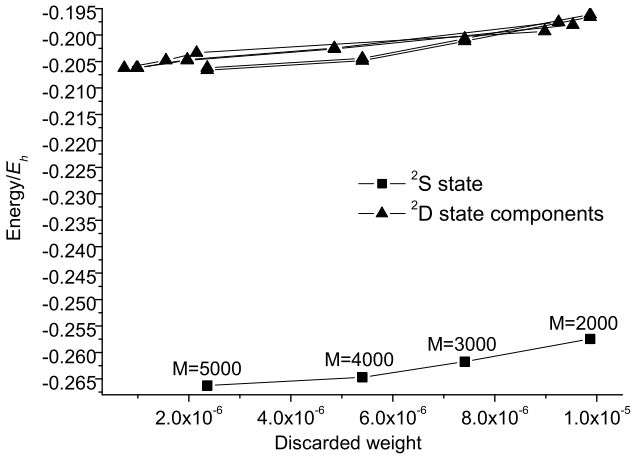

FIG. 3. Energy (E+18 994) in E_h and discarded weights of a spin-adapted DMRG calculation on the ^{2}S and ^{2}D states of the gold atom. Basis II.

TABLE II. The $5d^{10}6s^1$–$5d^96s^2$ energy separation in the Au atom (in eV); basis I.

Term	CASSCF-SO (11e,11o)	DMRG-SISO (43e,45o)[a]	Expt.[108]
Without SOC			
^{2}D	2.37	1.64	1.74
With SOC			
$^2D_{5/2}$	1.68	1.04	1.14
$^2D_{3/2}$	3.39	2.56	2.66
$^2D_{5/2}-{}^2D_{3/2}$	1.71	1.52	1.52

[a]Using state-averaged (11e,11o) CASSCF orbitals.

and $^2D_{3/2}$ states (corresponding to the $5d^96s^2$ configuration) was calculated using the ANO-RCC basis set contracted to 8s7p4d2f (basis I) and 8s7p5d3f (basis II). A state-averaged CASSCF calculation was carried out, as for the copper atom, with the same choice of weights for the ^{2}S and ^{2}D levels, including $5d$, $5d'$, $6s$ orbitals in the active space. Scalar relativistic effects were similarly taken into account at the CASSCF level using the second order Douglas-Kroll-Hess Hamiltonian.

In the subsequent DMRG calculations we kept the $1s$-$4p$ orbitals (i.e., a [Kr] shell) as frozen core and correlated all other orbitals; consequently, active spaces consisting of 45 and 57 orbitals were used for basis I and basis II,

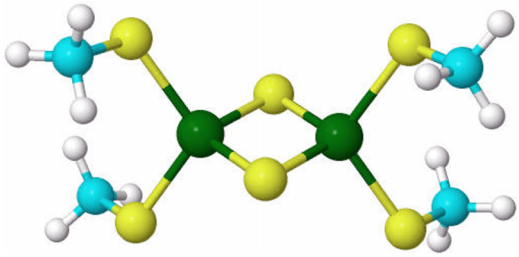

FIG. 4. The $[Fe_2S_2(SCH_3)_4]^{3-}$ molecule. The geometry is taken from Ref. 35.

respectively. The DMRG energy for each state was converged to about $10^{-3}E_h$ accuracy (energy differences to better than $10^{-3}E_h$ accuracy) using a bond-dimension of $M = 5000$ (see Figs. 2 and 3). The SO interaction matrix was then computed with the DMRG-SISO code. Table II shows the calculated and experimental data for basis I, while the results for basis II are shown in Table III.

For the gold atom we observe better agreement between state-averaged and state-specific CASSCF-SO calculations (see Table III). However, the CASSCF-SO calculations with the (11e,11o) active space, consisting of only valence orbitals with an additional $5d'$ set, do not provide wavefunctions of sufficient quality to compute the spin-orbit coupled energies to satisfactory accuracy. The computed $^2D_{5/2}$ and $^2D_{3/2}$ levels are 0.54 eV and 0.73 eV too high, respectively, with basis I, and 0.50 eV and 0.70 eV too high, respectively, with basis II.

The extended active spaces afforded by the DMRG (consisting of 45 and 57 orbitals) greatly improve on the (11e,11o) CASSCF description. In particular, the $^2D_{5/2}$ – $^2D_{3/2}$ splitting of 1.52 eV, obtained with the (43e,45o) DMRG-SISO using basis I, is in perfect agreement with the experimental splitting of 1.52 eV, compared to 1.71 eV from the initial (11e,11o) CASSCF-SISO calculation; for the $^2D_{5/2}$ and $^2D_{3/2}$ DMRG-SISO excitations are within 8% and 4% of the experimental energies, respectively.

For basis II we find good agreement with the results obtained in Ref. 53 with the same basis, and with experiment. In fact, we find that the (43e,57o) DMRG-SISO excitations are significantly closer to the experimental values than the (11e,11o) CASPT2-SO results, as the latter underestimates the position of the energy levels by 0.05-0.07 eV more than with the DMRG-SISO method.

TABLE III. The $5d^{10}6s^1$–$5d^96s^2$ energy separation in the Au atom (in eV); basis II.

Term	CASSCF-SO (11e,11o)	CASSCF-SO (11e,11o)[a]	CASPT2-SO (11e,11o)[a]	DMRG-SISO (43e,57o)[b]	Expt.[108]
Without SOC					
^{2}D	2.33	2.32	1.58	1.62	1.74
With SOC					
$^2D_{5/2}$	1.64	1.71	0.97	1.02	1.14
$^2D_{3/2}$	3.36	3.22	2.49	2.55	2.66
$^2D_{5/2}-{}^2D_{3/2}$	1.72	1.51	1.51	1.53	1.52

[a]State-specific CASSCF and CASPT2 from Ref. 53 using the same basis set.
[b]Using state-averaged (11e,11o) CASSCF orbitals.

TABLE IV. The low-lying states of $[Fe_2S_2(SCH_3)_4]^{3-}$. (Energies are in E_h.)

	S = 1/2		S = 3/2		S = 5/2	
M	Discarded weight	Energy	Discarded weight	Energy	Discarded weight	Energy
Case 1: *one state per S*						
1600	2.64×10^{-6}	−113.6819	2.01×10^{-5}	−113.6807	2.33×10^{-5}	−113.6800
2000	2.11×10^{-6}	−113.6824	1.55×10^{-5}	−113.6813	1.76×10^{-5}	−113.6805
Case 2: *two states per S*						
2000	9.31×10^{-6}	−113.6818	3.21×10^{-5}	−113.6806	3.63×10^{-5}	−113.6800
—		−113.6723		−113.6724		−113.6729

C. [2Fe – 2S] dimer

We now consider the $[Fe_2S_2(SCH_3)_4]^{3-}$ dimer, which is a model dimer for the [2Fe-2S] active sites in ferredoxins and other iron-sulfur proteins. We used the relaxed geometry from Ref. 35 (Fig. 4).

To determine a suitable active space, we first carried out an unrestricted BP86/TZP-DKH[109–111] calculation on the high spin state with $S_z = 9$. From the alpha and beta UKS orbitals we constructed unrestricted natural orbitals (UNOs). From the UNO occupations, the orbitals were separated into doubly occupied, singly occupied, and virtual molecular orbitals. Next, localized orbitals were constructed by projecting atomic orbitals into these 3 spaces (e.g., a localized core 1s orbital is obtained by projecting a 1s orbital into the doubly occupied space) followed by a subsequent orthonormalization. By population analysis and visualization of the projected AO's we determined a suitable active space. Our constructed active space consisted of 30 electrons in 36 orbitals, including (1) $3d$, $3d'$, $4s$ orbitals for Fe, (2) three $3p$ and two lowest-energy $3d$ orbitals on each bridging S atom, (3) one $3p$ orbital pointing toward the Fe atom on each ligand S atom.

We carried out DMRG calculations on 3 states with spin-multiplicities 2, 4, 6 (i.e., with $S = 1/2, 3/2, 5/2$) targeting only the lowest state (case 1) for each multiplicity, and targeting the two lowest states (case 2) for each multiplicity. The DMRG energies were converged to approximately $10^{-3}E_h$ accuracy with bond dimension $M = 2000$ (Table IV). No point-group symmetry was used.

According to Kramer's theorem, the doublet states cannot be split. The zero-field splitting for the first (lowest) quartet is small, −0.5 to 1 cm^{-1}, between two doublets, and the SOC lowers the average quartet energy, decreasing the doublet-quartet gap by 1-2 cm^{-1}. Similarly, the lowest sextet splits into three doublets, separated by ∼2 and ∼1 cm^{-1}, respectively (Table V). On increasing M and increasing the total number of states in the SISO calculation (case 1 versus case 2), the largest change is in the splitting of the levels *without* SOC; for example, the $S = 5/2$ state is lowered by 17 cm^{-1} on going from one to two $S = 5/2$ states in the DMRG calculation. This simply reflects that the energies are only converged to this accuracy with the chosen M. However, the pattern and magnitude of the ZFS remains very similar between case 1 and case 2 suggesting that the ZFS itself is reasonably well converged with respect to the number and quality of the SISO states. Interestingly, the ZFS of the second quartet and sextet states is much larger (25-35 cm^{-1}). This is a significant fraction of the Heisenberg exchange parameter, which is about 150 cm^{-1} in these systems.[112] This suggests that it can be relevant to consider SOC when fitting to a magnetic model Hamiltonian (Fig. 5).

TABLE V. The lowest states of $[Fe_2S_2(SCH_3)_4]^{3-}$ with SOC taken into account. (Energies are in cm^{-1}.)

M	Multiplet	Without SOC	SOC splitting
1600	S = 1/2	0	0
	S = 3/2	260.7	258.8 and 259.3
	S = 5/2	420.9	421.3, 423.1 and 424.1
Case 1			
2000	S = 1/2	0	0
	S = 3/2	241.7	240.0 and 240.4
	S = 5/2	409.0	409.5, 411.3 and 412.2
Case 2			
2000	S = 1/2 (I)	0	0
	S = 3/2 (I)	248.5	246.9 and 247.6
	S = 5/2 (I)	392.2	392.7, 394.1 and 395.0
	S = 1/2 (II)	2077.4	2125.7
	S = 3/2 (II)	2052.1	2034.3 and 2071.0
	S = 5/2 (II)	1943.7	1920.9, 1929.8 and 1945.3

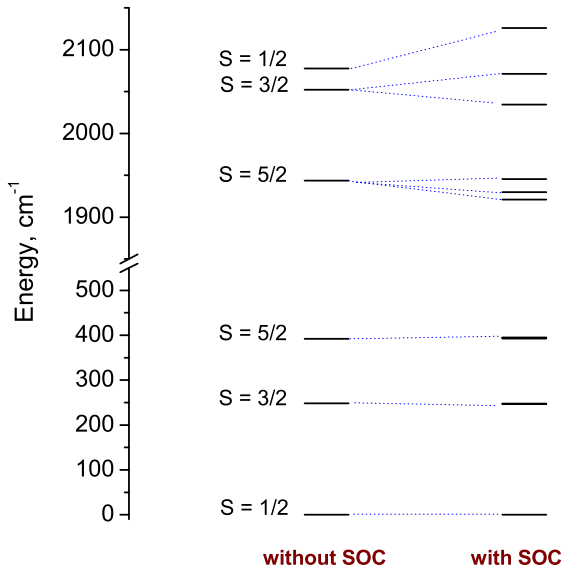

FIG. 5. Energy levels of $[Fe_2S_2(SCH_3)_4]^{3-}$.

IV. CONCLUSIONS

In this work, we described how to incorporate spin-orbit coupling effects into DMRG calculations within a state interaction spin-orbit framework. At the level of the spin-orbit mean-field approximation, the basic computation is to calculate transition density matrices between DMRG wavefunctions for different spin states. By far the largest cost of the procedure is in computing the individual DMRG wavefunctions for each spin state. We demonstrated the algorithm with benchmark calculations of zero-field splittings in the Cu and Au atoms, as well as in a model [2Fe-2S] complex, $[Fe_2S_2(SCH_3)_4]^{3-}$.

The prevalence of electronic degeneracies in transition metals means that the interplay between spin-orbit coupling and electronic correlations is potentially very rich. We see this in the [2Fe-2S] complex studied here, where we find that the zero-field splitting approaches the magnitude of the exchange coupling in the higher spin states. The ability of the DMRG to treat electronic structure in complexes with multiple metal sites, combined with the framework here for spin-orbit coupling, thus presents the new and exciting possibility to precisely determine the magnetochemistry of complicated transition metal systems.

ACKNOWLEDGMENTS

This work was supported by the US National Science Foundation, through the Award No. NSF:CHE-1265277.

[1]B. A. Heß and C. M. Marian, "Relativistic effects in the calculation of electronic energies," in *Computational Molecular Spectroscopy*, edited by P. Jensen and P. R. Bunker (John Wiley & Sons, New York, 2000), pp. 169–219.
[2]M. Reiher and A. Wolf, *Relativistic Quantum Chemistry* (Wiley, Weinheim, 2009).
[3]*Recent Advances in Relativistic Effects in Chemistry*, edited by K. Hirao and Y. Ishikawa (World Scientific Publishing, Singapore, 2004).
[4]*Relativistic Effects in Heavy-Element Chemistry and Physics*, edited by B. A. Heß (Wiley, New York, 2003).
[5]S. R. White and R. L. Martin, J. Chem. Phys. **110**, 4127 (1999).
[6]G. Fano, F. Ortolani, and L. Ziosi, J. Chem. Phys. **108**, 9246 (1998).
[7]A. O. Mitrushenkov, R. L. G. Fano, F. Ortolani, and P. Palmieri, J. Chem. Phys. **115**, 6815 (2001).
[8]G. K.-L. Chan and M. Head-Gordon, J. Chem. Phys. **116**, 4462 (2002).
[9]A. O. Mitrushenkov, R. Linguerri, P. Palmieri, and G. Fano, J. Chem. Phys. **119**, 4148 (2003).
[10]Ö. Legeza, J. Röder, and B. A. Heß, Phys. Rev. B **67**, 125114 (2003).
[11]Ö. Legeza, J. Röder, and B. A. Heß, Mol. Phys. **101**, 2019 (2003).
[12]Ö. Legeza and J. Sólyom, Phys. Rev. B **68**, 195116 (2003).
[13]Ö. Legeza and J. Sólyom, Phys. Rev. B **70**, 205118 (2004).
[14]G. K.-L. Chan, M. Kállay, and J. Gauss, J. Chem. Phys. **121**, 6110 (2004).
[15]G. Moritz, B. Hess, and M. Reiher, J. Chem. Phys. **122**, 024107 (2005).
[16]G. Moritz, A. Wolf, and M. Reiher, J. Chem. Phys. **123**, 184105 (2005).
[17]G. Moritz and M. Reiher, J. Chem. Phys. **124**, 034103 (2006).
[18]J. Hachmann, W. Cardoen, and G. K.-L. Chan, J. Chem. Phys. **125**, 144101 (2006).
[19]S. J. Rissler and R. M. Noack, Chem. Phys. **323**, 519 (2006).
[20]G. Moritz and M. Reiher, J. Chem. Phys. **126**, 244109 (2007).
[21]J. Hachmann, J. J. Dorando, M. Avilés, and G. K.-L. Chan, J. Chem. Phys. **127**, 134309 (2007).
[22]D. Ghosh, J. Hachmann, T. Yanai, and G. K.-L. Chan, J. Chem. Phys. **128**, 144117 (2008).
[23]G. K.-L. Chan, J. J. Dorando, D. Ghosh, J. Hachmann, E. Neuscamman, H. Wang, and T. Yanai, *Frontiers in Quantum Systems in Chemistry and Physics* (Springer, Netherlands, 2008), pp. 49–65.
[24]D. Zgid and M. Nooijen, J. Chem. Phys. **128**, 014107 (2008).
[25]D. Zgid and M. Nooijen, J. Chem. Phys. **128**, 144115 (2008).
[26]D. Zgid and M. Nooijen, J. Chem. Phys. **128**, 144116 (2008).
[27]Y. Ma and H. Ma, J. Chem. Phys. **138**, 224105 (2008).
[28]K. H. Marti, I. Ondík, G. Moritz, and M. Reiher, J. Chem. Phys. **128**, 014104 (2008).
[29]T. Yanai, Y. Kurashige, E. Neuscamman, and G. K.-L. Chan, J. Chem. Phys. **132**, 024105 (2010).
[30]H.-G. Luo, M.-P. Qin, and T. Xiang, Phys. Rev. B **81**, 235129 (2010).
[31]K. H. Marti and M. Reiher, Phys. Chem. Chem. Phys. **13**, 6750 (2011).
[32]G. Barcza, Ö. Legeza, K. H. Marti, and M. Reiher, Phys. Rev. A **83**, 012508 (2011).
[33]G. K.-L. Chan and S. Sharma, Annu. Rev. Phys. Chem. **62**, 465 (2011).
[34]Y. Kurashige and T. Yanai, J. Chem. Phys. **135**, 094104 (2011).
[35]S. Sharma and G. K.-L. Chan, J. Chem. Phys. **136**, 124121 (2012).
[36]K. Boguslawski, T. Tecmer, Ö. Legeza, and M. Reiher, J. Phys. Chem. Lett. **3**, 3129 (2012).
[37]S. Sharma, T. Yanai, G. H. Booth, C. Umrigar, and G. K.-L. Chan, J. Chem. Phys. **140**, 104112 (2014).
[38]S. Sharma, K. Sivalingam, F. Neese, and G. K.-L. Chan, Nat. Chem. **6**, 927 (2014).
[39]Y. Kurashige, J. Chalupsky, T. N. Lan, and T. Yanai, J. Chem. Phys. **141**, 174111 (2014).
[40]J. Chalupsky, T. A. Rokob, Y. Kurashige, T. Yanai, E. I. Solomon, L. Rulišec, and M. Srnec, J. Am. Chem. Soc. **136**, 15977 (2014).
[41]Y. Kurashige, G. K.-L. Chan, and T. Yanai, Nat. Chem. **5**, 660 (2013).
[42]S. Wouters and D. V. Neck, Eur. Phys. J. D **68**, 272 (2014).
[43]S. Wouters, T. Bogaerts, P. V. D. Voort, V. V. Speybroeck, and D. V. Neck, J. Chem. Phys. **140**, 241103 (2014).
[44]T. N. Lan, Y. Kurashige, and T. Yanai, J. Chem. Theory Comput. **11**, 73 (2015).
[45]S. M. Parker and T. Shiozaki, J. Chem. Phys. **141**, 211102 (2014).
[46]E. Fertitta, B. Paulus, G. Barcza, and Ö. Legeza, Phys. Rev. B **90**, 245129 (2014).
[47]S. Knecht, Ö. Legeza, and M. Reiher, J. Chem. Phys. **140**, 041101 (2014).
[48]Ö. Legeza, L. Veis, A. Poves, and J. Dukelsky, Phys. Rev. C **92**, 051303 (2015).
[49]W. Hu and G. K.-L. Chan, J. Chem. Theory Comput. **11**, 3000 (2015).
[50]S. Szalay, M. Pfeffer, V. Murg, G. Barcza, F. Verstraete, R. Schneider, and Ö. Legeza, Int. J. Quantum Chem. **115**, 1342 (2015).
[51]S. Keller, M. Dolfi, M. Troyer, and M. Reiher, J. Chem. Phys. **143**, 244118 (2015).
[52]R. Olivares-Amaya, W. Hu, N. Nakatani, S. Sharma, J. Yang, and G. K.-L. Chan, J. Chem. Phys. **142**, 034102 (2015).
[53]P.-Å. Malmqvist, B. Roos, and B. Schimmelpfennig, Chem. Phys. Lett. **357**, 230 (2002).
[54]A. Berning, M. Schweizer, H.-J. Werner, P. Knowles, and P. Palmieri, Mol. Phys. **98**, 1823 (2000).
[55]M. Sjøvoll, O. Gropen, and J. Olsen, Theor. Chem. Acc. **97**, 301 (1997).
[56]S. Yabushita, Z. Zhang, and R. M. Pitzer, J. Phys. Chem. A **103**, 5791 (1999).
[57]A. O. Mitrushenkov and P. Palmieri, Mol. Phys. **92**, 511 (1997).
[58]T. L. C. Jansen, S. Rettrup, C. R. Sarma, J. G. Snijders, and P. Palmieri, Int. J. Quantum Chem. **73**, 23 (1999).
[59]C. M. Marian, in *Reviews in Computational Chemistry*, edited by K. B. Lipkowitz and D. B. Boyd (Wiley-VCH, New York, 2001), Vol. 17, pp. 99–204.
[60]B. A. Heß, C. M. Marian, U. Wahlgren, and O. Gropen, Chem. Phys. Lett. **251**, 365 (1996).
[61]F. Neese, J. Chem. Phys. **122**, 034107 (2005).
[62]M. Roemelt, J. Chem. Phys. **143**, 044112 (2015).
[63]P. A. M. Dirac, Proc. R. Soc. London, Ser. A **117**, 610 (1928).
[64]G. Breit, Phys. Rev. **53**, 153 (1938).
[65]L. L. Foldy and S. A. Wouthuysen, Phys. Rev. **78**, 29 (1950).
[66]*Relativistic Electronic Structure Theory. Part 1. Fundamentals*, edited by P. Schwerdtfeger (Elsevier, Amsterdam, 2002).
[67]W. Pauli, Z. Phys. **43**, 601 (1927).
[68]G. Breit, Phys. Rev. **34**, 553 (1929).
[69]G. Breit, Phys. Rev. **39**, 616 (1929).
[70]M. Douglas and N. M. Kroll, Ann. Phys. **82**, 89 (1974).
[71]B. A. Heß, Phys. Rev. A **33**, 3742 (1986).
[72]G. Jansen and B. A. Heß, Phys. Rev. A **39**, 6016 (1989).
[73]A. Wolf, M. Reiher, and B. A. Hess, J. Chem. Phys. **117**, 9215 (2002).
[74]M. Reiher and A. Wolf, J. Chem. Phys. **121**, 2037 (2004).
[75]M. Reiher and A. Wolf, J. Chem. Phys. **121**, 10945 (2004).
[76]M. Reiher, Theor. Chem. Acc. **116**, 241 (2006).

[77]D. Ganyushin and F. Neese, J. Chem. Phys. **138**, 104113 (2013).
[78]M. Kleinschmidt, J. Tatchen, and C. M. Marian, J. Phys. Chem. **124**, 124101 (2006).
[79]M. Kleinschmidt and C. M. Marian, Chem. Phys. **311**, 71 (2005).
[80]D. Ganyushin and F. Neese, J. Chem. Phys. **125**, 024103 (2006).
[81]F. Neese and E. Solomon, Inorg. Chem. **37**, 6568 (1998).
[82]D. R. Yarkony, J. Chem. Phys. **84**, 2075 (1986).
[83]S. J. Havriliak and D. R. Yarkony, J. Chem. Phys. **83**, 1168 (1985).
[84]C. Teichteil, M. Pelissier, and F. Spiegelmann, Chem. Phys. **81**, 273 (1983).
[85]C. Teichteil and F. Spiegelmann, Chem. Phys. **81**, 283 (1983).
[86]D. G. Fedorov and J. P. Finley, Phys. Rev. A **64**, 042502 (2001).
[87]B. A. Heß, C. M. Marian, and S. D. Peyerimhoff, in *Modern Electronic Structure Theory*, edited by D. Yarkony (World Scientific, Singapore, 1995).
[88]C. M. Marian and U. Wahlgren, Chem. Phys. Lett. **251**, 357 (1996).
[89]D. Danovich, C. M. Marian, T. Neuheuser, S. D. Peyerimhoff, and S. Shaik, J. Chem. Phys. A **102**, 5923 (1998).
[90]J. Tatchen and C. M. Marian, Chem. Phys. Lett. **313**, 351 (1999).
[91]F. Neese, T. Petrenko, D. Ganyushin, and G. Olbrich, Coord. Chem. Rev. **257**, 288 (2007).
[92]A. Van Yperen-De Deyne, E. Pauwels, V. Van Speybroeck, and M. Waroquier, Phys. Chem. Chem. Phys. **14**, 10690 (2012).
[93]T. Helgaker, P. Jørgensen, and J. Olsen, *Molecular Electronic Structure Theory* (Wiley, Chichester, 2000).
[94]U. Schollwöck, Rev. Mod. Phys. **77**, 259 (2005).
[95]S. Östlund and S. Rommer, Phys. Rev. Lett. **75**, 3537 (2004).
[96]E. Cuthill and J. McKee, in *Proceedings of the 24th National Conference of the ACM* (ACM, 1969), pp. 157–172.
[97]J. Liu and A. Sherman, SIAM J. Numer. Anal. **13**, 198 (1975).
[98]I. P. McCulloch, J. Stat. Mech.: Theory Exp. **2007**, P10014.
[99]A. I. Toth, C. P. Moca, Ö. Legeza, and G. Zarand, Phys. Rev. B **78**, 245109 (2008).
[100]O. Vahtras, H. Ågren, P. Jørgensen, H. J. A. Jensen, T. Helgaker, and J. Olsen, J. Chem. Phys. **96**, 2118 (1992).
[101]M. J. Bearpark, N. C. Handy, P. Palmieri, and R. Tarroni, Mol. Phys. **80**, 479 (1993).
[102]H.-J. Werner, P. J. Knowles, G. Knizia, F. R. Manby, and M. Schütz, WIREs: Comput. Mol. Sci. **2**, 242 (2012).
[103]Q. Sun, http://sunqm.github.io/pyscf/.
[104]B. O. Roos, R. Lindh, P.-Å. Malmqvist, V. Veryazov, and P.-O. Widmark, J. Phys. Chem. A **109**, 6575 (2005).
[105]K. Pierloot, "Nondynamic correlation effects in transition metal coordination compounds," in *Computational Organometallic Chemistry*, edited by T. R. Cundari (Marcel Dekker, New York, 2001), pp. 123–158.
[106]T. H. Dunning, Jr., B. H. Botch, and J. F. Harrison, J. Chem. Phys. **72**, 3419 (1980).
[107]B. H. Botch, T. H. Dunning, Jr., and J. F. Harrison, J. Chem. Phys. **75**, 3466 (1981).
[108]J. E. Sansonetti and W. C. Martin, Handbook of basic atomic spectroscopic data, http://www.nist.gov/pml/data/handbook/index.cfm.
[109]A. D. Becke, Phys. Rev. A **38**, 3098 (1988).
[110]J. P. Perdew, Phys. Rev. B **33**, 8822 (1986).
[111]F. E. Jorge, A. C. Neto, G. G. Camiletti, and S. F. Machado, J. Chem. Phys. **130**, 064108 (2009).
[112]W. Gillum, R. Frankel, S. Foner, and R. Holm, Inorg. Chem. **15**, 1095 (1976).